HORIZON 2020
Research Infrastructures

H2020-INFRAIA-2014-2015
INFRAIA-1-2014-2015 Integrating and opening existing national and regional research infrastructures of European interest

ENSAR2
European Nuclear Science and Application Research 2
Grant Agreement Number: 654002

D9.6 – Summary of test results

Version: v2
Author: O Tengblad & F. Camera
Date: 20.07.2021

PROJECT AND DELIVERABLE INFORMATION SHEET

ENSAR2 Project Ref. №	654002
Project Title	European Nuclear Science and Application Research 2
Project Web Site	http://www.ensarfp7.eu/
Deliverable ID	D9.6
Deliverable Nature	Report
Deliverable Level*	PU
Contractual Date of Delivery	Month 66
Actual Date of Delivery	65
EC Project Officer	Mina Koleva

* The dissemination level is indicated as follows: PU – Public, PP – Restricted to other participants (including the Commission Services), RE – Restricted to a group specified by the consortium (including the Commission Services). CO – Confidential, only for members of the consortium (including the Commission Services).

DOCUMENT CONTROL SHEET

Document	Title: Summary of test results	
	ID: D9.6	
	Version	
	Available at: http://www.ensarfp7.eu/	
	Software Tool: Microsoft Word for Mac 2019	
	File: PASPAG-D9_6-v3.docx	
Authorship	Written by:	O. Tengblad and F. Camera
	Contributors:	P. Boutachkov, C. Mihai, A. Maj, J.A. Briz, V. García Tavora
	Reviewed by:	
	Approved by:	

DOCUMENT STATUS SHEET

Version	Date	Status	Comments
		For internal review	
		For internal review	
		Submitted on EC Participant Portal	
		Final version	

DOCUMENT KEYWORDS

Keywords	scintillators, gamma-detection, particle-detection, applications, p-CT imaging, SEE, Uranium enrichment

Disclaimer

Copyright notices

TABLE OF CONTENTS

LIST OF FIGURES

REFERENCES AND APPLICABLE DOCUMENTS

[1] Cholewa, M., Fischer, B. E. & Heiß, M. Preparatory experiments for a single ion hit facility at GSI. Nucl. Instrum. Methods Phys. Res. B 210, 296–301 (2003).

[2] O. Tengblad et al., Nuclear Instruments and Methods in Physics Research A 525 (2004) 458–464

[3] O. Tengblad et al., Nuclear Instruments and Methods in Physics Research A 704, (2013) 19–26.

[4] E. Nácher et al., Nuclear Instruments and Methods in Physics Research A 769 (2015) 105–111.

[5] Deans, Stanley R. (1983). The Radon Transform and Some of Its Applications. Nueva York: John Wiley & Sons.

[6] N. Chetih and Z. Messali, "Tomographic image reconstruction using filtered back projection (FBP) and algebraic reconstruction technique (ART)," 2015 3rd International Conference on Control, Engineering & Information Technology (CEIT), 2015, pp. 1-6, doi: 10.1109/CEIT.2015.7233031.

LIST OF ACRONYMS AND ABBREVIATIONS

LaBr	Scintillator crystal material, Ce doped: $LaBr_3(Ce)$
LaCl	Scintillator crystal material, Ce doped: $LaCl_3(Ce)$
Phoswich	Sandwich of two scintillator crystals with single readout
SiPM	Silicon Photo Multiplier
QDC	Charge to Digital Converter
ADC	Amplitude to Digital Converter
MDPPq	MESYTEC, 16 channel fast high resolution time and amplitude digitizer with QDC software
MVMLC	MESYTEC, FPGA-based VME Controller enabling VME module readout at high trigger and data rates.
SEE	Secondary Electron Emission
SEY	SEE yield
p-CT imaging	proton - Computer Tomography imaging
Derenzo	resolution phantom
PMMA	Poly (methyl methacrylate) (PMMA), also known as acrylic, acrylic glass, or plexiglass, standard material to make medical Phantoms

Executive Summary

The continuous development of our nuclear physics experiments demands for an extensive R&D to improve upon our equipment. These improvements, especially in scintillator materials has open up for many new cost-effective applications. Developments in scintillators materials, especially when detection of gamma-rays are involved, but, also the development in highly segmented Si-detectors can now be applied, both within our research and for the development of different societal applications.
The way forward departs form a detailed investigation of what we call a detector, i.e. the coupled device of a scintillator (and/or Si), its readout sensor (SiPM, photo tubes) and finally the signal digitalization. PASPAG has during these years investigated and advanced in all these ingrediencies.
In this report we present some new basic investigations on the combination of scintillators and sensors, we will discuss the final results from searching for nano-materials for secondary electron emission (SEE) investigations and a discussion on the R&D towards applications on p-CT imaging that has been performed within the PASPAG project.

Introduction

The PASPAG collaboration exploits novel scintillator materials and explores new techniques and concepts such as phoswich detectors and segmented or hybrid scintillators in order to simultaneously detect high-energy gamma rays, neutrons and charged particles. The emphasis has been modular approaches both in the scintillator crystals and photosensors as well as in the electronics with improved throughput and effective data processing allowing for compact scalable devices.

Technology out of basic science has been exploited for societal applications within the areas of nuclear medicine and homeland security. The characterization of new materials has been followed by the construction and testing of small-size prototypes and hybrid detectors for use in our scientific activity as well as for societal applications.

Section 1 Comparison of Coupling of LaBr with SiPM and with PhotoTube (INFN – F. Camera)

A $LaBr_3$(Ce;Sr) 3x3" crystal coupled to a matrix of 144 SIPM has been studied and compared to the same crystal coupled with a standard 3" PhotoTube. The SiPM-array is composed form of 6 x 6 mm^2 individual SiPM that together covers the full crystal (Fig. 1)

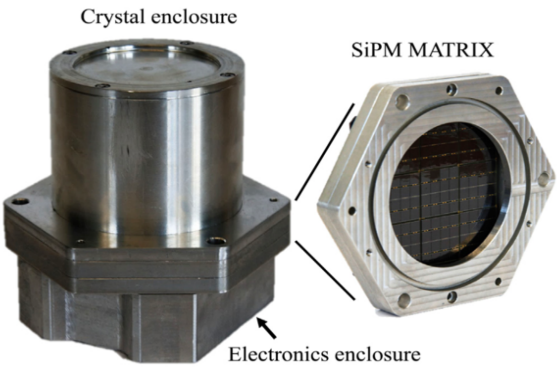

Figure 1: Photo of the $LaBr_3$(Ce;Sr) 3x3" crystal encapsulated and coupled to an array of 144 6x6mm^2 SiPMs.

In the case of the 144-SiPM array, for each event, both the individually measured signal by each SIPM and the total sum-signal of all 144 SiPMs, are recorded. First a comparison between the result using the SiPM-array and the standard PM tube was made. As can be seen from Fig. 2 the gamma ray resolution for ^{137}Cs and ^{60}Co source is the same in both cases.

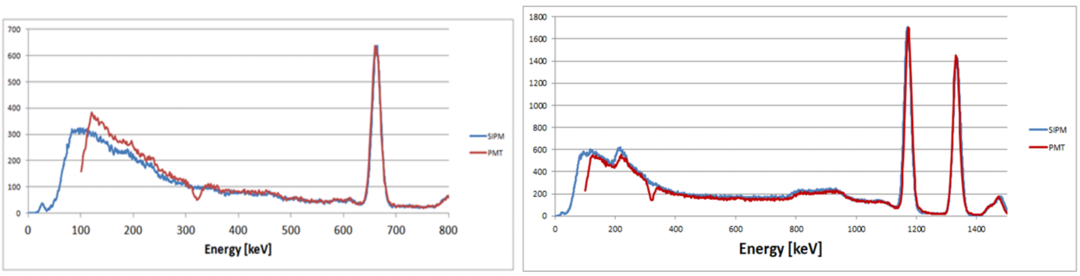

Figure 2: Gamma-ray spectrum from ^{137}Cs and ^{60}Co as measured by the LaBr3(Ce;Sr) 3x3" crystal coupled to a 3" PMtube (red) and to the SiPM-array (blue). The resolution (2.7 %) of the system is the same in both cases.

An interesting detail though, if one study the internal ^{227}Ac alpha-contamination, see Fig. 3, there is a shift in the alpha peak positions obtained when using the SiPM compared to the standard PM, a shift in the order 50 keV is observed. The crystal is the same so the reason must come from the sensors and have to be investigated further.

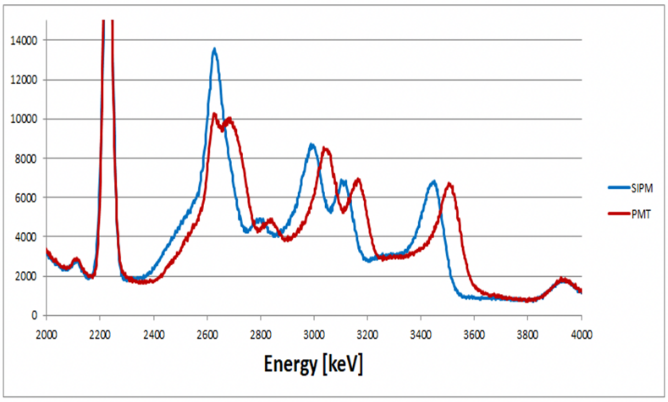

Figure 3: Spectrum obtain from the internal ^{227}Ac alpha contamination that is always present in $LaBr_3$ and $LaCl_3$ crystals. A shift in the order of 50 keV is observed, note that the gamma-ray peak though coincide perfectly.

Further, two types of studies were performed in order to see if it is possible to determining the position of the gamma-ray impact when using the SiPM array.

- Using a collimated ^{137}Cs source, placed so that the gamma ray-beam enter on the crystal in a definite x-y or z-y -position. (see Fig. 4.)
- Using a non-collimated ^{137}Cs source i.e. the full crystal is irradiated on its axis from a distance of approximately 20 cm. We call this measurement 'FLOOD'.

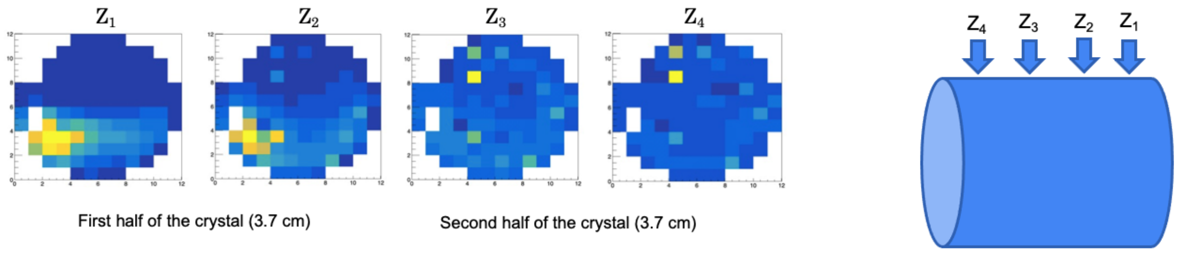

Figure 4: The figure shows the hit-patterns obtained when irradiating the crystal with gamma-rays from a collimated ^{137}Cs source at different positions along the Z-axis, the SiPM is mounted at Z_0.

In the spectra associated to the collimated source we notice that the spectrum measured by a single SIPM present a gaussian curve if it is far away from the collimation axis, while a tail appears to the right-side if it is near the collimation axis.

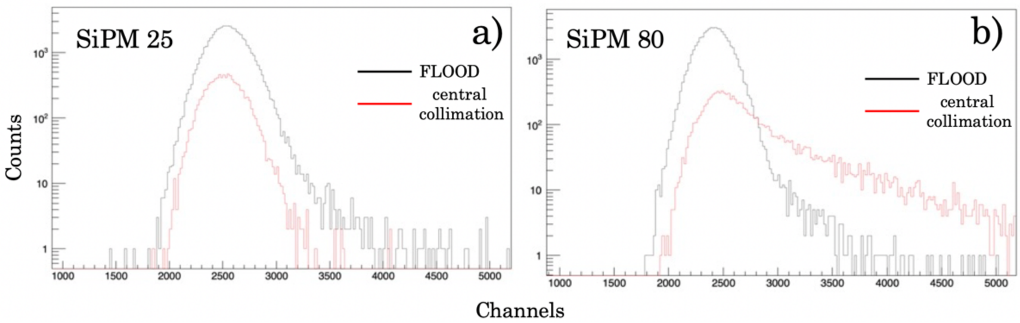

Figure 5: a) The SiPM located far from the collimation direction are expected to 'see' only the reflected light (red curve), while, b) the SiPM lying on the collimation direction are expected to detect a larger number of photons, as they are illuminated by direct light and by the reflected one (red curve).

Selecting events where the incident gamma-ray has deposited all its energy in the crystal the flood spectra measured by each SIPM is a gaussian with a centroid which depends on the quantum efficiency of the specific SIPM. A similar behaviour is also noticed on an event-by-event basis. However, in this case we cannot produce a spectrum as each SIPM provide a single number. We have therefore defined the observable 'd' , where x_i is the signal measured by SiPM ‘i’ and X^F and s^F are the centroid position and s extracted from a FLOOD measurement and then we can plot matrix with value of d measured by each SiPM.

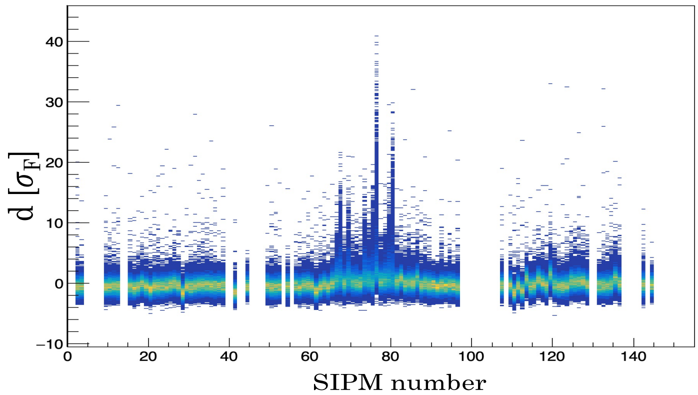

$$d_i = \frac{x_i - X_i^F}{\sigma_i^F}$$

Figure 6: The SiPM observable d as a function of the individual SiPM array-number.

Combining the data from Fig. 6 and Fig. 4 It is shown that we can localize the event if it happens near the SIPM but we cannot if it happens more than 4 cm away.

SECTION 2 DETECTING URANIUM ENRICHMENT USING $LaBr_3$(CE) COUPLED TO SIPM (IFIN-HH, C. MIHAI)

The same type of crystal (LaBr3(Ce;Sr) coupled with similar array of 56 SiPM (as mentioned in section 1) has been used as a prototype to be able to determine the enrichment of ^{235}U in a bulk ^{238}U sample. This is of course a very important application in order to be able to control and oversee the strategic use of nuclear reactors in different countries. From the results obtained, shown in Fig. 7, clearly illustrate that the prototype is sensible to the ^{235}U-enrichment of the sample especially that the 63.3 keV of ^{238}U and the 185 keV of ^{235}U lines are clearly identified and can be used to estimate the enrichment level.

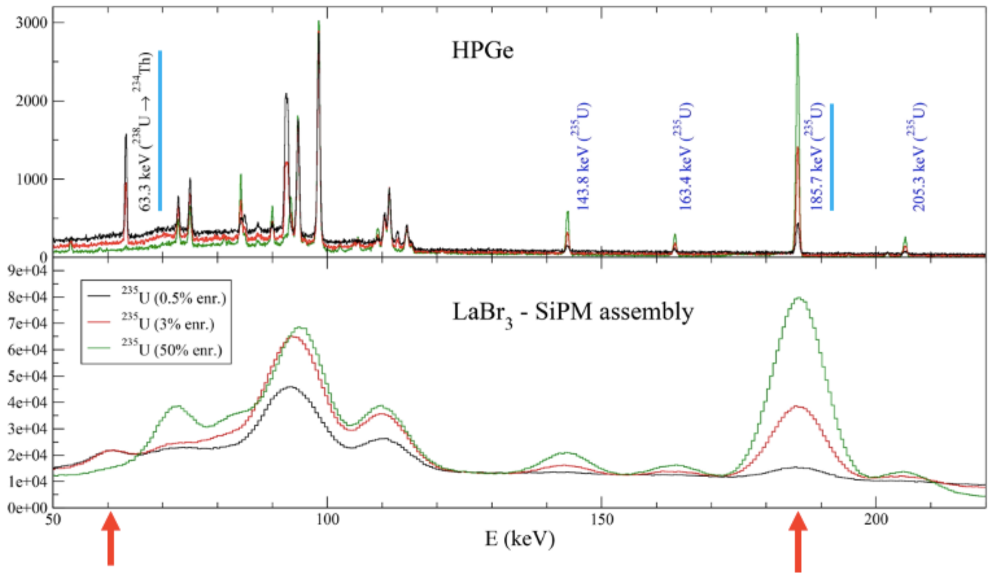

Figure 7: Spectra showing that the scintillator is sensible to the ^{235}U-enrichment of the sample and that the 63.3 keV of ^{238}U and the 185 keV of ^{235}U lines are clearly identified and can be used to estimate the enrichment level.

SECTION 3 NANO-MATERIALS WITH ENHANCED SECONDARY ELECTRON EMISSION (GSI – P. BOUTCHAKOV)

Stimulated electrons in the interaction of charged particles and radiation with matter which escape the material surface are called secondary electrons1. This secondary electron emission (SEE) is utilized in particle and radiation detectors2,3. The secondary electrons stimulated near the material surface have a better chance to escape the material, therefore nanomaterials may improve the SEE yield through the manipulation of material geometry. Further modification of the surface coating can be used to decrease the energy necessary for the electrons to leave the materials surface, further enhancing the SEE yield (SEY).
The purpose of this R&D is to find a nanomaterial that has a higher SEE than gold. A measurement of the SEE properties from 1D (one-dimensional) nanostructures of ZnO and ZnO/GaN (ZnO with GaN coating) composed of a mostly regular pattern of nanotubes grown on a thin Si3N4 substrate has been performed. A 4.77 meV/u Au beam. From the GSI UNILAC was directed to the microbeam experiment setup [1] .
ZnO nanotubes with a diameter of 1 µm and a length of 5 µm were employed for this research and the GaN was covered with 10 nm on the ZnO nanotubes. Additionally, a 20 nm Au deposited on thin (1 µm) silicon nitride (Si_3N_4) substrate sample was used as a reference/normalization (Fig. 8).

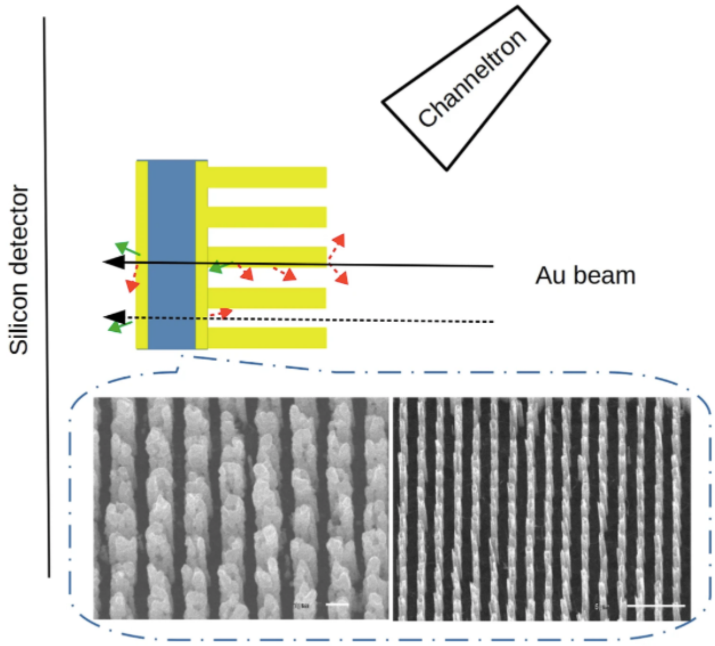

Figure 8: Schematic of the experimental setup. The insert shows SEM images of the investigated nanostructures: ZnO/GaN (left) with a scale of 1 µm and ZnO (right) with a scale of 5 µm. GaN coating was 10 nm thick and covered uniformly the top and side of nanorods and bottom of the Si_3N_4 film supporting the nanostructures.

The Au beam was focused to a ca. 0.1 mm beam spot. The heavy ions had sufficient energy, effectively penetrating the samples. The ions were stopped in a silicon surface barrier detector. A BURLE Electro-Optics channeltron Model 4028 was position 5 mm upstream from the target and a 180 V potential difference was applied between the sample surface and the channeltron, guiding the SEE electrons to the detector.

The Au ions pass through the sample and stop in the Silicon detector. The channeltron registers secondary electrons collected from the surface of the target. The secondary electrons are schematically depicted with red and green arrows. The green arrows symbolize δ-electrons, which can create further secondary electrons if they encounter the sample surface. In the inset, SEM pictures of the investigated nanostructures, to the left ZnO covered with GaN, and ZnO without coating to the right. The nanotubes, with spacing and diameters, are: 1.57 µm and 0.6–0.7 µm for the sample shown to the left; and 1.57 µm and 1–1.3 µm for the sample shown to the right. The approximate nanorod length is 5 µm, which is perpendicular to the surface.
The SEY spectrum obtained from the Au sample is shown at the inset of Fig. 9. The mean value of the distribution is proportional to the average number of secondary electrons created by a single gold ion passing through the sample. The area under the peak is equal to the number of ions which passed through the sample, while the distribution width is determined by the statistical processes involved in the creation of the SEY and their detection. Therefore, the two parameters of interest are the mean and width of the measured distribution.

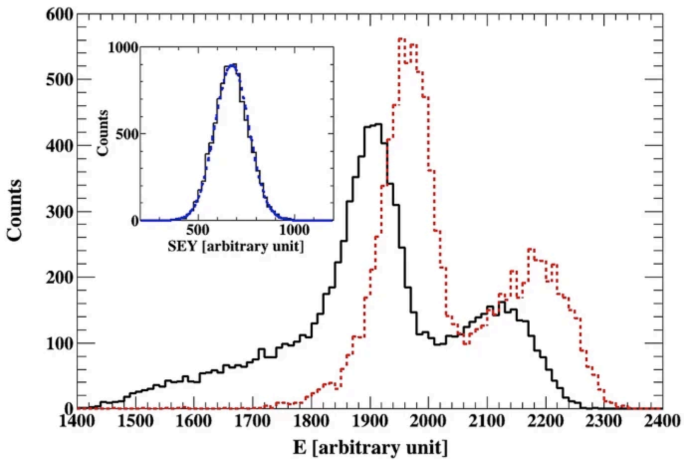

Figure 9: Energy spectrum measured by the Si detector for Au (red dashed line) and ZnO/GaN (black full line). The inset shows the secondary electron yield (SEY) measured by the channeltron, fitted by a normal distribution.

We can observe an average increase of 2.5 secondary electrons emitted from the 1D ZnO nanotubes compared to gold. The data also shows that GaN coating does not lead to a higher SEY yield.
One possible direction in future investigations is: (1) search for coating leading to larger SEY (2) investigating materials with smaller nano-tube diameter and larger density.
When considering thin detectors we suggest the use of a nanomaterial made by growing high aspect ridges on a thin substrate, with ridges regularly spaced and perpendicular to the substrate. If this material is placed at an angle relative to the beam, as illustrated in Fig. 10, the ions will pass through multiple ridges. Utilizing this approach, the SEY is increased due to passing through multiple surfaces. It is worth noting that presenting further surfaces due to the to the higher energy δ-electrons bumped by a neighboring nanostructure, the SEY will be further increased via secondary interactions with the material.

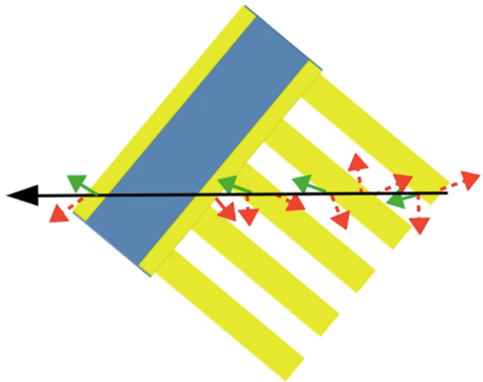

Figure 10: A concept of a nanostructure to increase the SEY per ion. The heavy ions depicted by the black arrow/line interact with the sample knocking slow electrons depicted in red, and δ-electrons depicted in green. A significant gain in the SEY is obtained due to passing through multiple entrance and exit surfaces.

The above research of the SEE properties of 1D nanomaterials could not fully answer the question: is the enhancement in the SEE properties a function of the nanostructure only or some other factors play important role? Therefore, a molecular beam of 1.5 MeV $^{+}H_2$ with a sub 70 nm resolution was used to investigate various 1D nanomaterials. The measurements were performed at the Centre for Ion Beam Applications (CIBA) at the National University of Singapore in Singapore and are under analysis.

In summary we have performed a comparison of SEE properties between novel nano-materials with one and three-dimensional nano-structures composed of a mostly regular pattern of rods. The nano-structured materials investigated show enhanced SEE properties when compared with gold (standard material used in SEE). Results from this work will enable the development of new radiation detectors for science and industry.

Full details of these investigations are published in the NATURE Scientific Reports:

https://www.nature.com/articles/s41598-020-80788-y
https://www.nature.com/articles/s41598-021-89990-y .

SECTION 4 PROTON-CT IMAGING PROTOTYPE (IEM – CSIC O. TENGBLAD, IFJ-PAN A. MAJ)

Proton- Proton-therapy offers great advantages with respect to the *X*-ray radiotherapy commonly used for cancer therapy. The main reason is that the largest energy deposited per unit length for a proton happens at the end of its path (Bragg peak). This behavior allows for a more selective treatment of tumors since higher dose is concentrated in the region where the proton stops, as well as less dose is deposited in the surrounding tissues as compared to radiotherapy with *X*- or γ-rays. Fig. 11 shows a comparison of the relative dose deposition using both radiotherapy techniques. The red region indicates the extra dose deposited in the body when using *X*-ray radiotherapy with respect to proton-therapy for a tumor located in the grey shadowed region. Proton-therapy is especially clean in comparison with *X*-rays radiotherapy for healthy tissues located deeper than the tumor to be treated and less damaging for tissues shallower than the tumor. A system of imaging and dose verification able to define effective treatments and to guarantee the correct location of the applied dose is mandatory. Currently, the treatment planning is guided via *X*-ray computed tomography (*X*-ray CT) images. Since the energy deposition by *X*-rays in matter differs from that of protons, the lack of accuracy in the estimation of proton ranges calculated using *X*-ray images is quite large (~3 %). Meanwhile, treatment plans made via proton-CT images will offer more accurate estimations and better control of the treatment. To this aim, we propose to perform medical imaging with proton beams via p-CT using particle detectors extensively used in Experimental Nuclear Physics. Those are the Double-Sided-Silicon-Strip-Detectors (DSSDs) [2].

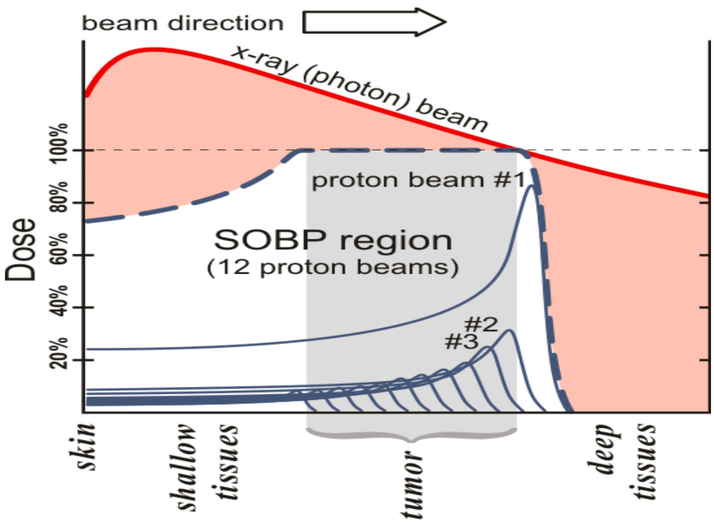

Figure 11: Comparison of absorbed doses for a radiotherapy treatment of a deep tumor using X-ray and proton beams. Red shadowed region indicates the extra dose deposited by X-rays with respect to proton beams for a value of 100 % required at the tumor location.

The DSSD detectors are a widely used type of silicon detectors with doubly strip structure allowing for the detection of the position of the incoming charged particle. It is structured with 16 horizontal times 16 vertical strips building a bi-dimensional mesh of 256 pixels of 3x3 mm^2. Using two of those detectors, one at the beam arrival (before the sample) and another one after passing through the sample allows to track the path of the proton. Furthermore, an additional detector to fully stop the outcoming protons is used as a residual energy detector. In this way, knowing the incident energy of the beam, the path (to estimate the effective length traversed of our sample) and the energy deposited in our detectors, we can estimate the energy lost in the sample. We can thus produce a map of energy losses vs horizontal and vertical positions to produce a spatial image of the sample. In order to test the validity of our methodology already performed a proof-of-concept test using a simpler experimental setup with low energy protons (~10 MeV) and 2-dimensional models at the tandem at CMAM (Madrid, Spain). The work of Monte Carlo simulations to optimize the setup, the data-taking and the analysis was the topic for two Master theses [2,3] defended (September 2019). We have continued these studies and tested our prototype with 3-dimensional models under more realistic conditions at the CCB facility Cracow Poland.

The residual energy detector is the CEPA4 detector [3, 4]. It is composed by an array of 2x2 detectors each of them in phoswich configuration: $LaBr_3$ (4 cm) + $LaCl_3$ (6 cm) with a common readout. It offers good capabilities for detection of protons up to 300 MeV and gamma rays of up to 10 MeV with good efficiency and energy resolution. These properties make it suitable for pCT imaging as residual energy detector.

The first measurements were performed summer 2019 using simple-thin-2D phantoms of less than 1-mm-thick at the 5 MV tandem accelerator in CMAM (Madrid). A 10-MeV proton beam was scattered in a bismuth target reducing the beam intensity and irradiating our full sample continuously (Fig. 12). Successful results were obtained by using only 2 DSSD detectors usually dedicated only for tracking but, in this case, due to the low-energy of the beam used, the second detector was also acting as a residual energy detector. The former experiment was a successful test of the tracking system and associated electronics. We had two master students making their final theses-work on the preparations, simulations and execution of this experiment.

https://www.iem.cfmac.csic.es/departamentos/nuclear/fnexp/reports/TFM/TFM-Posadillo_de_Bringas.pdf & https://www.iem.cfmac.csic.es/departamentos/nuclear/fnexp/reports/TFM/TFM-V_Tavora.pdf

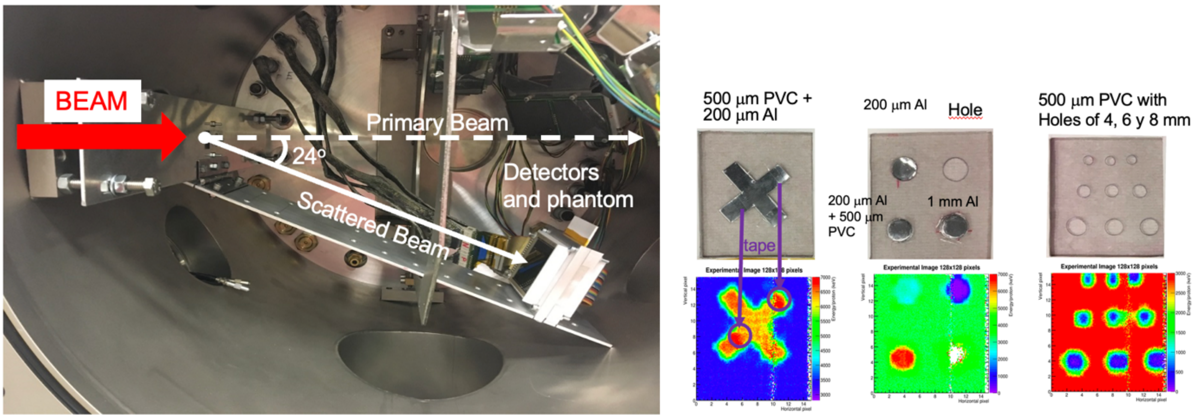

Figure 12: To the left the experimental setup at CMAM; 10 MeV protons scattered on Bi, the the 1mm thin phantoms sandwiched between 2 DSSDs. To the right; top row shows the phantoms, and the bottom row the experimental data.

The hands-on activity was stopped due to the confinement restrictions placed by covid-19 in 2020. However, design, simulations and preparation for a prototype in order to perform a more realistic test using 3D phantoms of 6 -10 cm depth and using, apart from the tracker detectors also one specific detector for the measurement of residual energy were continued, now with a new technician Vicente Garcia Tavora employed (1.10.2020 – 30.08.2021) on the PASPAG project. Also, this year (2021) we have taken extra help from 3 master-students working on the prototype experiment. One performing GEANT4 simulation to optimize the setup to better understand the results. A second who did the pre-experimental tests as preparation of the setup for the experiment in Krakow and is now performing the data analysis,

and the third student is testing different algorithms and optimizing the tomographic image reconstruction. The three master-theses are to be delivered and defended in September 2021.
The experimental setup is shown schematically in Fig. 13; A scattering target (made of titanium) was used in order to reduce the incident proton beam intensity down to a level for the detectors to properly work (~1 kHz). A stable intensity of ~1 nA (100 & 110 MeV) proton beam impinging on the experimental setup, the detectors were placed at a scattering angle of ~12 degrees and a distance of 1 meter from the target.

As mentioned above, a set of 2 DSSD detectors used as proton trackers placed before and after the phantom are required for the tracking of incoming outgoing protons for the imaging reconstruction.

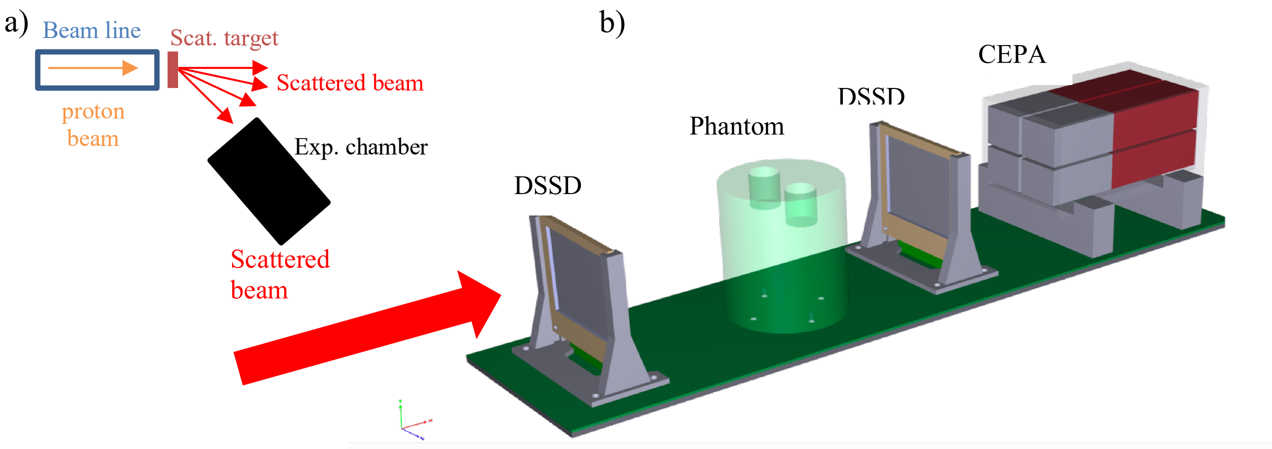

Figure 13: Sketch of the experimental setup. a) General view of the setup, including a scattering target to be located at the exit of the CCB beamline. The experimental chamber located at an angle of -30º and distance of 1.5 m from the scattering target impinged by the proton beam. b) Main components in the experimental chamber. The scattered beam traverses the particle tracker detectors (DSSD1 and DSSD2), the sample to be imaged (phantom) and finally fully stopped in the CEPA4 detector.

In order to test the prototype, phantoms with different geometries, insert patterns, spatial distributions of inserts, were used. To test the spatial resolution, a Derenzo-type 3D phantom (basically a cylinder with holes of different diameters and distances) was used. For the 3D reconstruction method, the measurements were performed rotating the phantom via a remotely controlled rotatory disk taking samples every x degree. By using the reconstruction algorithms, the CT image of the 3D volume of the phantom is explored by transversal cuts to evaluate the properties of the reconstructed image.

For the preparation of the experiment, Monte Carlo simulations were performed using the GEANT4 code. In those simulations, several orientations, relative distances among our detectors and the phantom and different beam energies have been evaluated. As an example, two different geometries corresponding to two different phantoms to be studied are shown in Fig. 14. Preliminary results from the GEANT4 studies are shown in Figure 15. There, the image shown on the left side is obtained for the cross-pattern phantom shown in Fig. 14-left. The image on the right side is a preliminary reconstruction using a simple Filtered Back Projection algorithm with the projections taken with the two-insert phantom (shown are testing different advanced algorithms and improvements in order to obtain more detailed images in order to evaluate the image properties.

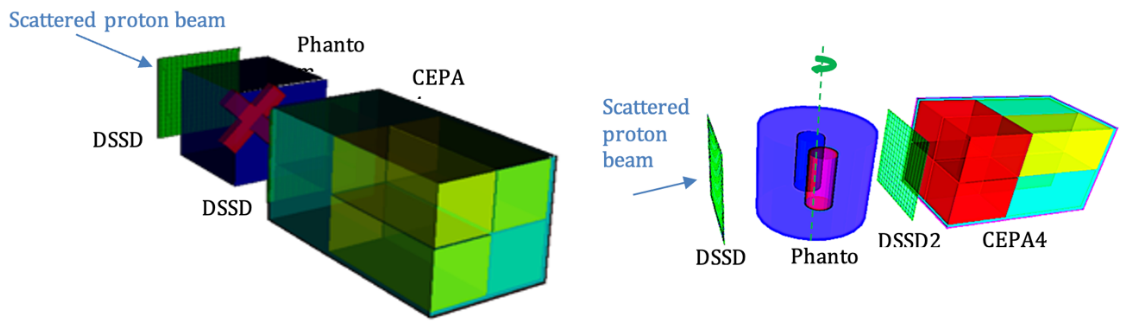

Figure 14: Geometry of the experimental setup as included in Geant4 simulations. Two different phantoms are shown. The cross shaped (red) aluminum inserts on a PMMA cubic matrix shown on the left used to take a simple projection to evaluate the image. The PMMA phantom with inserts of Alcohol and Water shown in the right sketch was evaluated at several rotation angles in order to reconstruct the pCT image of the phantom from the projections acquired.

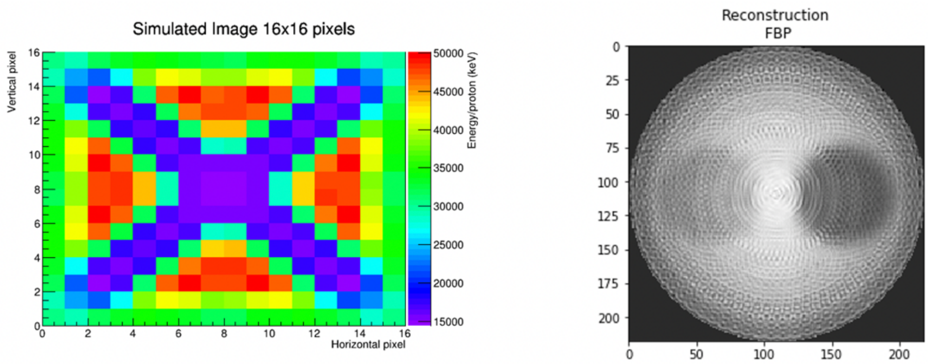

Figure 15: Images obtained using Geant4, simulating the two different geometrical patterns of the phantom shown in Figure 14-left using a proton beam of 100 MeV. The left image corresponds to a cross-shaped insert in the phantom, and the right image is the result obtained using the Filtered Back Projection reconstruction algorithm for the phantom with two-inserts (alcohol-water).

The experimental setup as shown in the photo of Fig. 16 was fully assembled and tested in our Laboratory at IEM in Madrid.

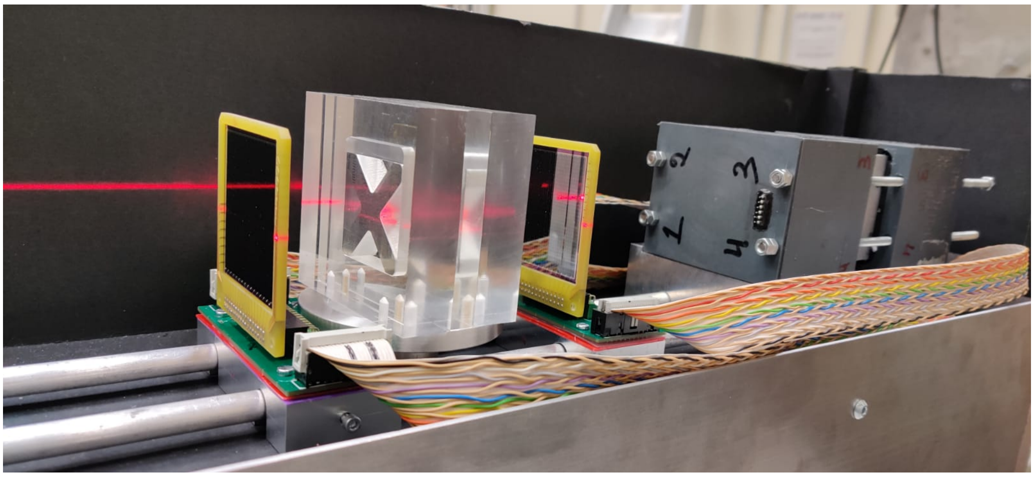

Figure 16: The experimental set up used at Centrum Cyklotronowe Bronowice (Kraków, Poland) June 4-7, 2021, not shown is the cover, as the Si detectors have to be in full darkness.

The experiment could finally be performed in June 2021. The equipment was shipped from Madrid to Krakow and 3 researchers followed to mount and perform the experiment with participation and help from our collaborators of IFJ PAN and financial support from ENSAR2 access.
The experiment details @ Centrum Cyklotronowe Bronowice (Kraków, Poland) in June 4-7, 2021, are summarized below and in the Fig. 17;

Detectors:

- 1x Scintillator-Array of 4 LaBr3 (20x20x30 mm3) (CEPA4)
- 2x Double Sided Striped Silicon Detectors (1 mm)

Electronics & DAQ:

- Mesytec – MVMLC VME controller and readout
- Mesytec – MDPPq-16ch digitizer for the CEPA4 PM-tube signals (4x anode + 4 last dynode)
- Mesytec – 4x (MPR-16ch preamp + STM-16ch) amplifier for treating the 2x DSSD signals (64)
- CAEN – 2x V785 ADC-32ch for digitizing the DSSD signals
- Minicomputer running linux and the Mesytec mvme Open-source VME data acquisition system

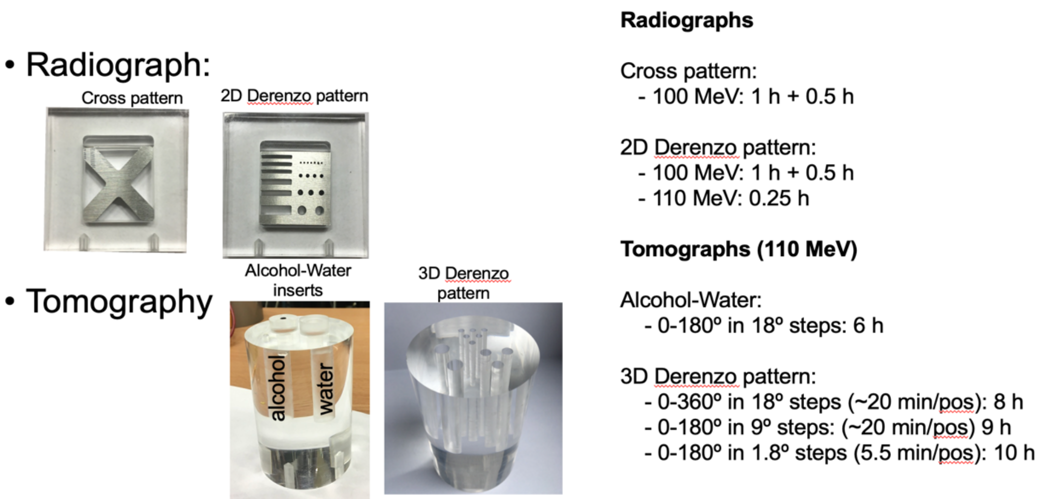

Figure 17: Details from the data taking at Centrum Cyklotronowe Bronowice in June 2021. The different phantoms, beam energies and measurement times are shown.

An example of the on-line raw data from the radiography measurement of the cross-pattern is shown in Fig. 18

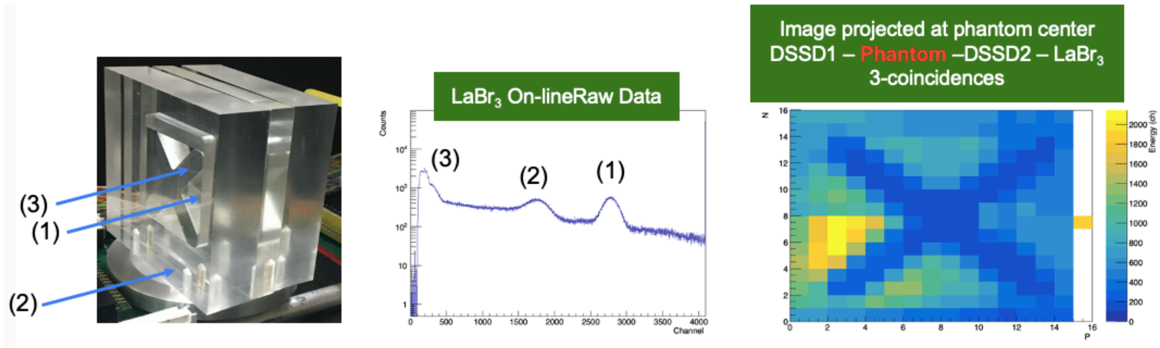

Figure 18: On-line raw-data form the pattern measurement; from left to right: a) the PMMA phantom irradiated by 100 MeV protons, b) Online spectra in the Scintillator Array: 3 peaks corresponding to protons that gone through: 1) PMMA(20) + AIR(10) + PMMA(20mm) 2) PMMA(50mm), and 3) PMMA(20) + Al(10) + PMMA(20mm). c) To the right; the reconstruction under triple Coincidence conditions; DSSD1 + DSSD2 + LaBr3 detector.

The data-analysis is on-going, but the preliminary results are already excellent as can be seen from Fig. 19. One can appreciate an improvement when increasing the number of projections made, and when reducing the step size from 18^O to 9^O, also, to make a full 360 degrees turn seems redundant. In this case, Radon transform [5] and the Filtered Back Projection (FBP) [6]was used to obtain the result.

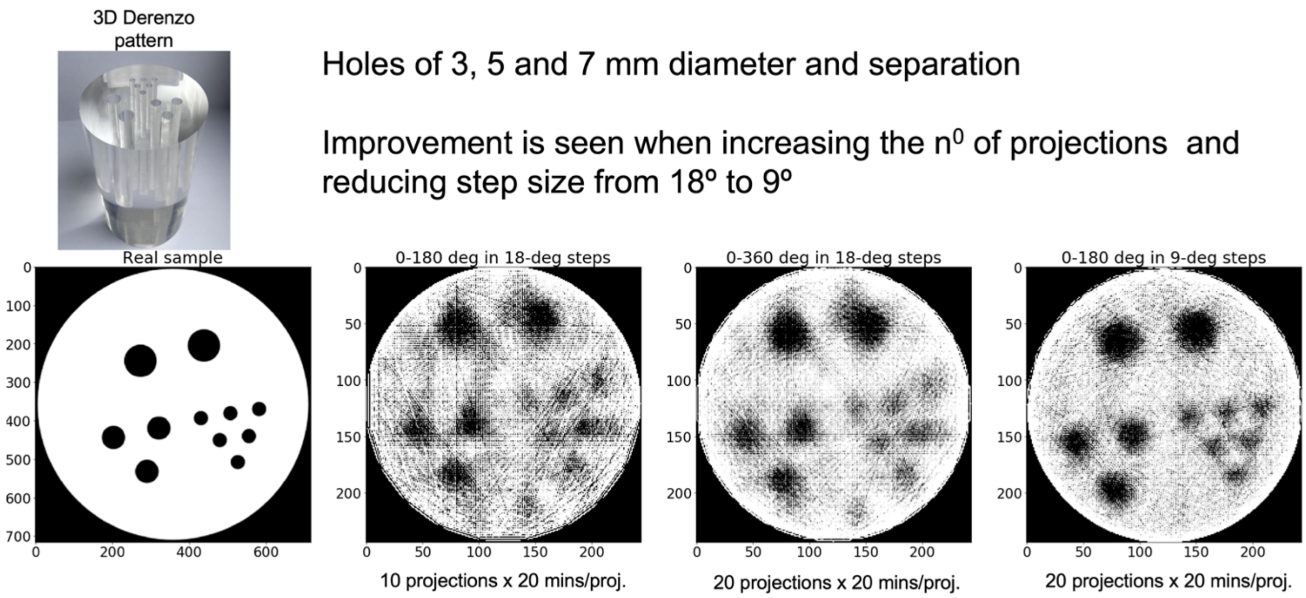

Figure 19: On top is shown the 3D-derenzo phantom (PMMA) used in the experiment. To the left is shown the real sample, followed by the reconstruction result from the different measurements made.

SECTION 5 PUBLICATIONS AND OUTREACH

Sub-Section 5.1 Published papers:

Boutachkov, P., Voss, K.O., Lee, K. et al. An investigation of secondary electron emission from ZnO based nanomaterials for future applications in radiation detectors. Sci Rep 11, 737 (2021). https://doi.org/10.1038/s41598-020-80788-y

Cholewa, M., Cappellazzo, M., Ley, M. et al. In search of nano-materials with enhanced secondary electron emission for radiation detectors. Sci Rep 11, 10517 (2021). https://doi.org/10.1038/s41598-021-89990-y

Sub-Section 5.2 Conference contributions and Outreach

Developing a prototype of pCT scanner.
III Jornadas RSEF/IFIMED de Física Médica 2020. 14-15 December 2020. Oral Contribution
https://indico.ific.uv.es/event/5983/contributions/13890/

Testing a pCT scanner prototype: first tests
The 7th International Conference on Advancements in Nuclear Instrumentation Measurement Methods and their Applications (ANIMMA 2021). 21-25 June 2021. Poster Contribution with Intensive Oral presentation + Conference Proceedings.
https://indico.utef.cvut.cz/event/23/

PASPAG web. https://www.iem.cfmac.csic.es/departamentos/nuclear/WEB-PASPAG/webstyle1/

Sub-Section 5.3 Master Theses

- María Inmaculada Posadillo de Bringas: Desarrollo de un prototipo con DSSDs para realizar imagen médica con protones. University of Sevilla, Spain 10/09/2019
  https://www.iem.cfmac.csic.es/departamentos/nuclear/fnexp/reports/TFM/TFM-Posadillo_de_Bringas.pdf

- Simulaciones Monte Carlo para el desarrollo de un prototipo de tomo ́grafo de protones con aplicación en protonterapia. University of Sevilla, Spain 10/09/2019
  https://www.iem.cfmac.csic.es/departamentos/nuclear/fnexp/reports/TFM/TFM-V_Tavora.pdf

Master theses in preparation for September 2021.

- Pedro Martínez Moreno: Reconstrucción de imágenes tomográficas del prototipo de escáner pct del IEM. University of Complutense Madrid, Spain
- Carlos Ballesteros Bejarano: Estudio de capturas radiográficas de fantomas gruesos empleando el prototipo de escáner de protones del IEM-CSIC. University of Complutense Madrid, Spain
- Amanda Nerio: Experimental tests of a scanner prototype for medical imaging with protons @ IEM-CSIC. University of Complutense Madrid, Spain

CONCLUSION

Within the PASPAG collaboration several studies of new promising scintillator materials have been performed. These new materials have been characterized with gamma rays and charged particles. This investigations and comparisons of material and sensors and different couplings have led to prototyping actual performing detectors.

In this final deliverable D9.6 we summarize some of the test results of very promising prototype detectors. We have shown that with specialized algorithms we can combining the right scintillator with the best readout sensor determining the interaction point of gamma-ray radiation and thus obtain a detector with directional sensitivity that is of outmost interest for directional detecting movement of radioactivity in a crowd of people e.g., at a transfer hall of an airport. We have shown another application where we can determine the ^{235}U enrichment in bulk ^{238}U samples that is of highest importance to observe and control if international agreements on the composition of fuel for nuclear reactors are being followed.

We have also shown very promising results of a prototype for p-CT imaging. Our R&D will not stop here even though the ENSAR2 is coming to an end. In the case of p-CT imaging we already have beamtime approved to further improve of the prototype and to move towards even bigger phantoms and higher proton energies to fully match with the actual clinical situation.